Characterization of the summer surface mesoscale dynamics at Dome F, Antarctica.

Sergi Gonzalez[1], Francisco Vasallo[1], Pablo Sanz[2], Antonio Quesada[3], Ana Justel[4]

[1]Antarctic Group, Spanish Meteorological Agency (AEMET), Spain

[2]Centro de Computación Científica, Universidad Autónoma de Madrid, Madrid, Spain

[3] Department of Biology, Universidad Autónoma de Madrid, Spain

[4] Department of Mathematics, Universidad Autónoma de Madrid, Spain

Abstract

This article characterizes the mesoscale surface air temperature (SAT) gradients around the Dome F on the Antarctic Plateau combining ERA5 reanalysis outputs and in-situ weather observations. For this we took advantage of a mobile automatic weather station (M-AWS) that allowed us to record meteorological observations in interesting areas not covered by other AWS. We found that night-time SAT gradients are very variable from night to night. ERA5 does not adequately represent thermal gradients and their daily changes and tends to underestimate them. In particular, it fails to reproduce the cold pool observed by M-AWS over the depressed areas of the terrain. The performance of ERA5 over the plateau is better when observed SAT gradients are weak. Besides, we observed surface meso-β eddies with warm cores and horizontal gradients of more than 5 ˚C $100km^{-1}$ simulated by ERA5 that have implications for site selection to establish new telescopes for astronomical observations. This study helps to interpret the daily performance of SAT values provided by reanalyisis on the Antarctic Plateau and complements climatological evaluations of SAT in the region. Finally, this study raises the necessity to increase in-situ weather observations, not only on the ridges of the Antarctic plateau where the majority are located, but also in the areas of depression to have a better picture of the weather and climate of the plateau.

Keywords: Antarctic Plateau, weather observations, mesoscale dynamics, cold pools, surface air temperature

1. Introduction

The East Antarctic Plateau is the coldest place on Earth. It is the highest area of the Antarctic ice-sheet that rises to about 3000 m in height on the eastern side of the continent, east of the Transantarctic Mountains. A ridge with three domes, Dome C (75° 06’S, 123 ° 20’E, 3233 m), Dome A (80° 22’S, 77° 21’E, 4093 m), and Dome F (77° 19’S, 39° 42’E, 3810 m) crosses the plateau from the Australian sector to the African sector. The terrain is mostly homogenous with little roughness (<0.5 m) and falls slightly from the ridges with very gentle slopes (<0.5 degrees) (Markus et al., 2017). Near the coast, the downward slope increases and leads to lower terrain with a contrasting milder climate.

Cold temperatures and downslope winds are the meteorological features that best characterize the climate over the Antarctic Plateau (Allison et al., 1993; Kikuchi et al., 1992). In winter cold katabatic winds dominate, descending perpendicular to the height levels and increasing with angle of the slope, turning anticlockwise due to the Coriolis force (Parish and Bromwich, 2007). In summer, the blocking effects of the Antarctic terrain produce the same wind pattern (Parish and Cassano, 2003; van den Broeke and van Lipzig, 2003). Therefore, winds are slight over the plateau and are mighty near the coast. Mean annual surface air temperatures (SAT) vary with altitude, reaching -30 °C to -35 °C over the dome in summer and -60 °C to -70 °C in winter, the later characterized by a coreless winter, that is, nearly constant temperatures between May and September (Allison et al., 1993; Thompson, 1969). The lowest SAT on Earth was measured at the Vostok station, with -89.2 °C (Turner et al., 2009).

Although the plateau presents a smooth orography, the temperature does not follow a simple lapse rate. This can be illustrated by the comparison of two long record stations, Dome Fuji and Vostok. Dome Fuji station is 300 m higher than Vostok station, and despite of this, the latter has a lower mean annual SAT (Yamanouchi et al., 2003). This difference may be caused by the surface topography that leads to cold air stagnation near the Vostok basin (Yamanouchi et al., 2003). Indeed, a lower SAT than the record measured in Vostok have been observed in topographic depressions using satellite imagery (Scambos et al., 2018; Surdyk, 2002).

This fact provides evidence that the Antarctic Plateau is not as thermally homogenous as the orography of the ice sheet could suggest. However, due to the inaccessibility and the harsh conditions, few weather stations operate over the plateau. This prevents the detection of possibly interesting small-scale transient structures and horizontal gradients in SAT. High-resolution meteorological reanalysis and models can fill this gap. However, such data must be validated using observational records to establish its reliability and limitations (Gallée and Gorodetskaya, 2010; Vignon et al., 2018). In fact, this region has been identified as an optimal location for new AWS in order to improve the Antarctic meteorological network (Hakim et al., 2020). Most of the studies and verifications previously carried out focus on large climatological series using annual, seasonal or monthly means (*e.g.* Allison et al., 1993; Dabberdt, 1970; Kikuchi et al., 1992; Yamanouchi et al., 2003) or in the study of the vertical regime of the atmospheric boundary layer (ABL; e.g. Argentini et al., 2005; Genthon et al., 2010; Hudson and Brandt, 2005; Vignon et al., 2017), and they leave out mesoscale structures and gradients.

In this article, we analyse some small-scale temperature structures combining data from meteorological reanalysis and measurements made by different automatic weather stations (AWS), including a mobile automatic weather station (M-AWS) carried on-board a zero emissions polar vehicle (Gonzalez et al., 2019). The mobility of the M-AWS is an advantage in order to study small scale variability and horizontal gradients in a scarcely-observed place like the Antarctic Plateau. The objective of this study is to validate different reanalyses on an hourly and daily scale and to analyse the capacity of the state-of-the-art reanalyses to reproduce transient and small-scale meteorological structures such as nocturnal cool pools. Finally, we characterize the different small-scale features found at the Antarctic Plateau under different meteorological settings. In section 2 we describe the area of study. Data and methods used are described in section 3. A statistical validation of the reanalysis used is shown in section 4. In section 5 the horizontal temperature gradients and small scale structures on the Plateau are characterized. Finally, we draw some conclusions in section 6.

2. Area of study

The area of study is the African sector (in the Dronning Maud Land) of the Antarctic Plateau Ice Sheet around Dome F (Fig. 1). This area is characterized by elevations over 3000 m altitude, and very gentle slopes smaller than 0.5º. The area culminates in the Dome Fuji at 3810 m. For clarity, in this article we distinguish between the region that we call “Dome F” or simply “dome”, and the highest point of the dome and the AWS located there that we call “Dome Fuji”. From the Dome Fuji, a ridge extends to the northwest and acts as the ice divide between the ice flowing to the Filchner-Ronne Ice Shelf and that flowing to the Atlantic and Indian sectors of the Southern Ocean. On this ridge the JASE2007 AWS is located at 391 km from Dome Fuji. Another ridge extends to the northeast, dividing into two drainaige basins. Finally, a third ridge extends to the southeast of the Dome F connecting with Dome A through a saddle point on the ridge.

Low-level climate in the area is characterized by very low temperatures. The monthly mean SAT at Dome Fuji are found between -35 °C in December and -66 °C in May (Yamanouchi et al., 2003). Studies performed with fixed AWS settled at the north-east ridge of the Dome Fuji by the

Japanese Antarctic Research Expedition (JARE) found that SAT decreases almost constantly with altitude (Takahashi et al., 1998). In summer below 3000 m, monthly mean surface lapse rates are similar to the adiabatic lapse rate (1 °C $100m^{-1}$). Lapse rate increases in winter, especially at high elevations. Near the top of the Dome, the mean annual surface lapse rate is higher, around 1.5 °C $100m^{-1}$, and presents a large monthly variability, ranging from 0.3 °C to 3 °C $100m^{-1}$. Sudden and abrupt warmings are occasionally observed in the area as a result of warm air advection produced by persistent blocking highs over East Antarctica (Enomoto et al., 1998; Hirasawa et al., 2013).

The region is characterized to be an area of wind divergence (Parish and Bromwich, 2007). The wind is weak at the Dome Fuji and does not have a predominant direction (Yamanouchi et al., 2003). High-resolution simulations indicate that katabatic winds develop at the downslopes of the region and accelerate with the slope to the coast (Parish and Bromwich, 2007). However, such katabatic forcing is considerably weaker during the summer period in which we focus on. From December to February, diabatic solar heating on the ice sheet disrupts the surface cooling reducing the presence of the katabatic forcing over the plateau. Instead, the blocking effect of the orography of the continent produces a wind configuration similar to that of the katabatic wind regime (Parish and Cassano, 2003; van den Broeke and van Lipzig, 2003).

Atmospheric boundary layer (ABL) height observed at Dome C shows a daily cycle in summer varying from 20-100 m at night to 150-300 m during the day (Argentini et al., 2005; Genthon et al., 2010; Hudson and Brandt, 2005). In this season, nocturnal inversions often exceed 1 °C in 10 m building a strong wind shear on the surface that decouples the stable ABL layer from the free-atmosphere aloft (Genthon et al., 2010; Vignon et al., 2017). Daytime convective eddies at the ABL produced by incoming solar radiation 'resets' the nocturnal stratification of the ABL from one night to the following (Vignon et al., 2017). Those conditions observed at Dome C are expected to occur also at Dome F.

3. Data and Methods

3.1 Data

3.1.1 Observations

We installed a M-AWS (Mobile Automatic Weather Station) on board a zero-emissions Windsled vehicle (Gonzalez et al., 2019) that followed a 2538 km transect around the African sector of the Plateau in the 2018/19 austral summer, coinciding with the Year of Polar Prediction in the

Southern Hemisphere Special Observing Period (YOPP-SH SOP; Bromwich et al., 2020; Jung et al., 2016). The route started on the plateau near Novolazárevskaya station at 3150 m and approached Dome Fuji reaching to 3745 m (Fig. 1b). M-AWS recorded half-hourly near-surface georeferenced observations of temperature and humidity from 18 Dec 2018 to 1 Feb 2019, but no wind speed nor direction were observed. Data was complemented with information of observation of the clouds and the present weather (*e.g.* snow, diamond dust, fog, etc.) logged by the expedition members after training. Weather observation notes were made once a day by filling in a table specially designed for this expedition (Fig. S1).

For the same period, hourly near-surface temperatures were available from two fixed automatic weather stations (AWS), Dome Fuji and JASE2007, both operated by Japan (Fig. 1b). Dome Fuji AWS is located at the top of the Dome F at 3810 m, next to the homonymous Japanese research station. JASE2007 is located 390 km at northwest of the Dome Fuji station, over the ice divide at 3661 m. The only other station in the area is Relay AWS, located 379 km at north of the Dome Fuji station at 3353 m, at the edge of the Plateau. It was not used in this study because it remains far away from the transect of the M-AWS. Only three stations cover this vast area, and due to the harsh environment and logistic limitations it is unlikely that new stations would be installed in the near future. Furthermore, there is a lack of data about the conditions at the topographic depressions since all the stations are settled on a ridge of the terrain.

M-AWS did not collect data for the temperature series between 27 Dec 2018 at 16:30 UTC and 5 Jan 2019 at 0:30 UTC. Both fixed stations (JASE2007 and Dome Fuji) did not collect data in short periods during the expedition. The missing values caused temporary discontinuity, but due to their irregular occurrence they did not introduce relevant biases in the averages. Therefore, we considered unnecessary to reconstruct the series by interpolation.

The main concern about the observational data is the warm bias experimented at the diurnal hours by the solar radiation (Genthon et al., 2011). Due to the high-power consumption required by aspirated shields, the temperature probes in Antarctica are often housed in naturally ventilated radiation shields. This causes overheating when the sun is high and the wind speed is low. A quality control of the data should be performed using wind speed to avoid these warm spikes (Genthon et al., 2011), but the M-AWS did not record wind data. Instead, a statistical quality control was performed to detect possible outliers. We analysed the behaviour of the reanalyses in each hour of the daily cycle by calculating the average of the biases produced by the reanalyses when approximating the observations. To isolate the possible effect of solar radiation on the measurement of temperatures in the AWS, we compared the biases of each pair of reanalyses with data from the central hours of the night (21:00, 00:00 and 03:00 UTC).

We used the paired t-test with Bonferroni correction for pairwise comparisons (at the 0.05 level of global significance).

Unlike what occurs with the Dome Fuji data, the temperature observations recorded by the M-AWS were not assimilated in the reanalyses and therefore constitute independent measurements to perform the evaluation.

3.1.2 Reanalysis

Due to the few observations available in Antarctica, reanalyses are a tool often used to study the meteorology of the continent. State-of-the-art reanalyses are physically and dynamically coherent and they cover the lack of observations with information from many other sources, such is the satellite data (Dee et al., 2014). However, the lack of observational data leads to increased sensitivity of the reanalysis to the model internal dynamics that may lead to large biases in high-latitude regions (Gossart et al., 2019). In particular, considerable biases has been observed in the SAT over Antarctic Plateau with a pronounced warm bias, especially in the winter season (Bracegirdle and Marshall, 2012; Fréville et al., 2014; Jones and Lister, 2015) that are still present in ERA5 (Gossart et al., 2019). SAT is a diagnostic variable computed using interpolations and parametrizations of the surface fluxes (ECMWF, 2009). This scheme works quite well in mid-latitudes, but performes worse at low temperatures and under strong static stratification (Atlaskin and Vihma, 2012). Three reanalyses have been considered in this study: ERA5, MERRA-2 and ERA-Interim.

ERA5 (Hersbach et al., 2020) is the 5th generation global climate reanalysis of the ECMWF. It has a horizontal resolution of 31 km on 137 hybrid levels. It produces analysis fields at hourly intervals for a number of parameters from 1950 to the present day. ERA5 is based on the IFS Cycle 41r2 of the ECMWF implemented in 2016 with 4D-Var data assimilation, coupled to a soil model. It also includes a ten-member ensemble with reduced resolution.

MERRA-2 (Gelaro et al., 2017) is the global climate reanalysis of the GMAO and it is based on the version 5.12.4 of the GEOS atmospheric data assimilation system. It has a horizontal resolution of 0.5° x 0.65° on 72 hybrid levels. Analysis fields are produced every 6 hours using a 3D-Var data assimilation. The data extends back to 1980. Compared to the previous version, it includes assimilation of aerosol observations and improvements of cryospheric processes and stratospheric ozone.

ERA-Interim (Dee et al., 2011) is the predecessor of ECMWF ERA5 and it uses the IFS Cycle 31r2 released in 2006. We used it because is still frequently used in the literature and for the sake of comparisons with previous studies. The data is assimilated using the 4D-Var technique. The horizontal resolution is approximately 80 km (T255 spectral) on 60 hybrid levels. The surface parameters have been gridded with a time resolution of 3 hours, available from 1 Jan 1979 to 31 Aug 2019.

To compare the values of the different reanalyses with the observations recorded by the three AWSs in the 2018/19 austral summer, the nearest grid point to each AWS location was obtained. Due to the differences between the model and AWS elevation can be considerable, an adjustment in temperature should be performed to obtain comparable results. Different techniques have been applied for this step, either using the dry adiabatic lapse-rate (Tetzner et al., 2019; Zentek and Heinemann, 2020) or using the lapse rate of the neighbouring grid cells (Gossart et al., 2019). In this study we decided to use near-surface lapse rate (lapse rate of SAT at different elevations of the terrain; Navarro-Serrano et al. (2018)) of the area [70˚ S 90˚ S 10˚ W 55˚ E] measured by ERA5, that is 7.5 ˚C 100 m^{-1}. The largest corrections made were 0.36 ˚C for ERA5, 0.73 ˚C for MERRA2 and 0.80 ˚C for ERA-Interim. Fig. S2 shows the hourly SAT measured by all three AWSs and the corresponding values of ERA5, MERRA-2 and ERA-Interim at the same locations.

3.2 Methods

3.2.1 Statistics

For the M-AWS data, the statistical quality control to detect outliers was carried out with the method of Chen & Liu (1993) for time series. Additive outliers were identified using the R software package tsoutliers (https://cran.r-project.org/package=tsoutliers) with automatic selection of the ARIMA model (López-de-Lacalle, 2019). The search was performed separately on the two main sections of the M-AWS data, before 28 Dec 2018 and after 5 Jan 2019, finding one and two additive outliers, respectively. These are the temperatures recorded on 26 Dec at 23:00, 12 Jan at 6:00 and 17 Jan at 13:00. These data were removed for statistical comparison of the reanalyses with the M-AWS.

Linear regression models were fitted to assess the ability of the three reanalyses to reproduce temperature observations in the study area of the Antarctic Plateau. We analysed whether the data evidenced that there was a statistically significant relationship between the temperatures provided by the models and the observations (t-test for slope equal to zero in the null), and whether the reanalysis reproduced the same temperatures (t-test for slope equal to one in the null). To evaluate the performance of ERA-5, MERRA-2 and ERA-Interim reanalyses, the temperature values they provided at the locations of the three AWS were compared to the observations using the mean absolute error (MAE), BIAS and Pearson correlation coefficient.

Moreover, we analysed the behaviour of the reanalyses in each hour of the daily cycle by calculating the average of the biases produced by the reanalyses when approximating the observations. To isolate the possible effect of solar radiation on the measurement of temperatures in the AWS, we compared the biases of each pair of reanalyses, on the one hand with data from the central three hours of the night (21:00, 00:00 and 03:00 UTC), and on the other with those of the day (9:00, 12:00 and 15:00 UTC). We used the paired t-test with Bonferroni correction for multiple comparisons (at the 0.05 level of global significance).

3.2.2 Case Studies

Case studies examined in section 4 were analysed by combining information from observations and ERA5 reanalysis outputs. The synoptic setting is described using the temperature and geopotential height at 500 hPa in ERA5, where it is expected that the large-scale features at mid-to-upper-levels do not differ much from the reality. To describe the surface conditions in ERA5 we used the 2m temperature and the wind field. Temperatures and horizontal temperature gradients between stations were compared using the nearest grid point to each station. As explained in Section 2.1, the maximum daily SAT measured by AWS may be overestimated due to solar radiation overheating. For this reason, in the case studies, we focused on the study of the minimum temperatures (defined as the minimum temperature between 21:00 and 03:00 UTC) that are not subjected to this warm bias. The minimum temperature was used instead of the temperature at one specific time (e.g. at 00:00 UTC) because the changes of temperature are so rapid that a difference of one hour on reaching the minimum temperature may imply a difference of few degrees. Since our intention is to characterize the cool pool and not the exact timing, the minimum temperature is a more suitable variable. The vertical structure (atmospheric soundings and cross sections) of the low atmosphere was also examined using the temperature, specific humidity and wind output in ERA5 at model levels and calculating the equivalent potential temperature.

4. Statistical validation of reanalysis in the African sector of the Antarctic Plateau during the SH-YOPP SOP

The relationship between the observations and the temperature values provided by the reanalyses at the locations of the three AWS at each time are shown in Fig. 2a, separately for ERA5, MERRA-2 and ERA-Interim. There is a significant linear relationship between the values provided by the reanalysis and the temperatures recorded by the AWSs (all p-values << 0.0001). However, the temperatures cannot be considered coincident since all slopes were significantly different from 1 (p-value << 0.0001). The slope values that most closely approximated to 1 were those of MERRA-2 (0.67) and ERA5 (0.61). Intercepts of linear models were also similar with -13.3 for ERA 5 and -12.04 for MERRA-2. The Pearson correlation coefficients were 0.84 for both ERA5 and MERRA-2. For ERA-Interim, the slope was 0.56, the intercept was -11.9 and Pearson correlation coefficient was 0.89. Linear fits for each reanalysis with data from each AWS separately provide very similar results (Fig. S3 and Table 1).

When comparing the differences between the values provided by the reanalysis and those observed in the three AWS, the MAE varied between 2.33 °C in ERA-Interim and 3.16 °C in MERRA-2. ERA-Interim featured the smallest BIAS with only +0.66 °C that explains the best MAE. After a bias correction of the data, the MAE was nearly the same across all reanalyses, ranging from 2.3 to 2.4 °C (not shown). When we look in more detail at the proportion of reanalysis data that differ by more than 5 °C from the observations, we see that it is higher in MERRA-2 (19%) than in ERA5 (15%). Both reanalyses showed a cold bias with -2.05 °C in ERA5 and -2.49 °C in MERRA-2 (Table 1 and Fig. 2b), indicating that they tended to underestimate a significant part of the AWS observations. Fig. 2c shows that ERA5 was the reanalysis that tended to underestimate higher temperatures. ERA-Interim behaved differently, overestimating 6% of the data by more than 5 °C, almost all below -30 °C (Fig. 2c), and only underestimating 2% by more than 5 °C.

When the variation of the temperatures throughout the day was analysed for the three reanalyses, relevant patterns were observed according to the AWS (Fig. 3). At night, the averages of the temperatures provided by ERA5 corresponded well with those of the observations recorded by the three AWS, with differences less than 2 °C. In the same hours MERRA-2 also reproduced well the temperatures recorded by M-AWS and JASE2007 but it provided lower temperatures than in Dome Fuji, with a bias of up to 4 °C. The discrepancies were more evident in the middle hours of the day when the underestimation of the temperature also occurred with

MERRA-2 and ERA5 compared with all AWS. The hourly performance of ERA-Interim was the opposite, as the greatest differences occurred at night while daytime temperatures were very similar to those observed in the three AWS. During the night, ERA-Interim provided higher temperatures than observed, with an average difference from the M-AWS observations of almost 4 degrees.

The underestimation of temperatures observed during the central hours of the day with ERA5 and MERRA-2 was compatible with the overheating of the temperature probes. Therefore, with the available information, it was not possible to discern whether these were due to overheating or systematic biases of the models. However, as the minimum daily temperatures occurred at night when the solar radiation was not heating the sensor, they can be used to analyse the meteorology of the region on a daily scale. During the night, ERA-Interim showed substantial warm bias (Table 1). Although overall ERA5 and MERRA-2 were generally quite similar, the performance of the reanalyses in the representation of the daily cycle was dependent on AWS. In the central hours of the night and day, the biases of all the reanalyses differed significantly (p-values $\ll 0.0001$), except ERA5 and MERRA-2 in JASE2007 (p-values 0.135 and 0.55) and in the M-AWS (p-values 0.035 and 0.041, above the significance level with Bonferroni correction). However, MERRA-2 showed large differences in the BIAS of the three stations. The underestimation of the temperature by almost 2 °C during the night with MERRA-2 in Dome Fuji made ERA5 the most consistent option for analysing daily changes and case studies that occurred in the region.

5. Small-scale structures over the Plateau

The statistical validation provides a large-scale overview of the ability of the reanalysis to simulate the SAT at different points and the general strengths and weaknesses they have. However, this kind of validation does not provide detailed information on how the reanalyses reproduce the dynamics over the plateau and the temperature gradients or possible transient small-scale structures formed in determined events. To investigate both aspects, in this section, we analyse different cases combining ERA5 reanalysis outputs and in-situ observations. We also discuss the performance of ERA5 to simulate the daily SAT changes and gradients over the area of study.

5.1 Temperature gradients and cool pools around the ice divide during stable conditions

Fig. 4 shows the SAT and the weather observations made by the M-AWS and the Dome Fuji AWS and the ERA5 reanalysis at their locations between 7 and 23 Jan, when the M-AWS was moving around the Dome F. The diurnal cycle dominates throughout the period. The synoptic signal such as warm or cold advections modulates the diurnal cycle by warming or cooling the air with respect to the previous day. This is the case of the 18-20 Jan when a cold advection occured (Fig. 4). However, such modulations are limited and temperatures are influenced by other factors. Wind speed is also important in modulating temperatures. Wind at night increases turbulence in the nocturnal boundary layer by mechanical forcing. The turbulence generates a heat flux in the stratified boundary layer that compensates radiative cooling at the surface (Van de Wiel et al., 2012). This is exemplified in the night of 14-15 Jan, when the increase in wind at Dome Fuji caused a significant increase in the minimum temperature and a reduction in the thermal amplitude of the day. As discussed earlier, midday temperatures are very sensitive to shield heating; therefore, we will not discuss them in this section. We focus on nocturnal horizontal gradients and how they change around the ice divide.

During the period between 7 and 23 Jan, ERA5 presented a positive bias in the minimum SAT at night (Table S1). Night-time bias during this period was larger than the mean bias during the campaign (Table 1). However, the bias was uneven among stations. While Dome Fuji presented an average difference of only 0.5 ˚C with ERA5, JASE2007 and the M-AWS presented an average difference of about 2.1 ˚C and 2.5 ˚C, respectively. We also calculated the horizontal gradient between the M-AWS or JASE2007 and Dome Fuji (the highest point in the area). The average gradient between JASE2007 and Dome Fuji was -0.2 ˚C $100km^{-1}$, consistent with the negative near-surface adiabatic lapse-rate then considering the difference in height (149 m). On the contrary, the mean gradient between the M-AWS and Dome Fuji was positive with 1.1 ˚C $100km^{-1}$. Although the M-AWS was moving at different altitudes during this period, this value indicates that it might be more subjected to cool pools than JASE2007 during this part of the transect. The gradients computed with the SAT simulated by the ERA5 reanalysis are also positive in the case of JASE2007 and negative in the M-AWS, but differ considerably with the magnitude (-0.6 ˚C $100km^{-1}$ between JASE2007 and Dome Fuji and 0.2 ˚C $100km^{-1}$ between M-AWS and Dome Fuji).

After examining all the daily changes of nocturnal temperatures (Table S1) we found that horizontal SAT gradient at meso-α scale (~500 km) is highly variable, even under stable conditions. The gradient between Dome Fuji and JASE 2007, separated by 391 km, often change more than 1 ˚C 100km^{-1} in 24 hours subjected to small variations of the synoptic conditions (Video S1 and S2). This makes it difficult for ERA5 to consistently reproduce those SAT variations, which are sometimes missing by more than 1 ˚C 100km^{-1}. The variations between Dome Fuji and M-AWS are even greater, but here the change in the location of the vehicle has to be considered.

To analyse why the temperature gradients differ and how ERA5 reproduces them, we focused on few days studied in more detail. The interest of these days lies in the fact that the path travelled by the Windsled that transports the M-AWS crossed the two sides of the saddle between Dome F and Dome A. This saddle is important in terms of temperature gradients, as this region has a higher occurrence of thermal emission surface temperature <-90 ˚C than the top of the Dome Fuji (see Fig. 1 in Scambos et al., 2018). Therefore, it is a region affected by cool pools during winter, and possibly also during summer nights. We chose days without major advections that allowed us to observe the effect of the saddle on the night-time temperatures, and the ability of the ERA5 to reproduce the horizontal gradients over this area (Table 2).

6-7 Jan 2019

On the night between 6 and 7 Jan 2019, Dome F was under a shallow anticyclone with a geopotential of 5000 gpm and -34 ˚C at 500 hPa (Fig. S4a). On 7 Jan 2019 at 00:00 UTC (Fig. 5a), ERA5 simulates a SAT between -33 and -36 ˚C in the area comprising the three stations. SAT generally decreases with height at the dome. However, near the Dome Fuji station, a mesoscale anticyclonic vortex encircled an area with higher SAT of approximately 50 km in diameter (see Section 4.3). Measurements at 00:00 UTC indicate -33.1 ˚C at Dome F and -34.6 ˚C at JASE2007, which reached -35.2 ˚C overnight. The higher SAT of Dome Fuji relative to JASE2007 can be produced by the vortex observed in the ERA5. However, the M-AWS, which is located at the same altitude than JASE2007 but on the western side of the saddle, measured a much lower value of -38.0 ˚C, producing a horizontal gradient of temperature of 2.7 ˚C 100km^{-1}. That difference is not well reproduced by ERA5 which provided a minimum temperature of -34.7 and a gradient of around 0.1 ˚C 100km^{-1}. A possible explanation for this disparity could be due to the fact that the cool pool descending from the saddle is not well captured by the reanalysis.

11-12 Jan 2019

Few days later, on 12 Jan 2019 at 00:00 UTC a very deep midlatitude ridge entered the continent from the Kemp Land (Fig. S4b). The ridge had a geopotential of 5120 gpm over the Dome F and advected warm air of -28 ˚C at 500 hPa from NE. That day the M-AWS reached the top of the saddle. The SAT in the area according to ERA5 (Fig. 5b) was lower than in the previous case (between -35 and -38 ˚C in the area between the Dome Fuji and the M-AWS), and the lowest temperatures were not centred over the Dome F but over the Dome A and the saddle. The difference between the warm temperatures at 500 hPa and the cold temperatures near surface created a very strong inversion layer at low levels (Fig. S5), completely decoupling the surface weather and the mid-level synoptic regime. The temperature simulated by ERA5 at the location of the M-AWS approximates the observation (-37.8 ˚C recorded in M-AWS vs. -37.0 simulated; Table 2). Dome Fuji and JASE2007 recorded minimum temperatures of -36.1 and -26.2 ˚C respectively. Therefore, the horizontal gradient between M-AWS and Dome Fuji was 0.7 ˚C 100km^{-1}, similar to the corresponding value in ERA5 (0.9 ˚C 100km^{-1}). All weak gradients (< 1 ˚C 100km^{-1}) between M-AWS and Dome Fuji took place from 8 to 14 Jan, with the sole exception of the 12-13 night which increased to 1.4 ˚C 100km^{-1} (Table S1). During this period, the observed and simulated gradients agreed quite well compared to the rest of the period. However, temperatures in ERA5 were not close to observations, but the biases at the two stations had the same sign and similar magnitude. Temperatures increased importantly toward the coast but the observed gradient between Dome Fuji and JASE2007 (-2.5˚ C 100km^{-1}) was significantly higher than in ERA5 (-1.5˚ C 100km^{-1}).

13-14 Jan 2019

During the next two days, the ridge closed into an isolated anticyclone that remained almost stationary over the Dome F for few days (Video S1). On the night between 13 and 14 Jan 2019, the anticyclone had a geopotential of 5160 gpm and a warm core of -29 ˚C to the SW of Dome Fuji at 500 hPa (Fig. S4c). During the previous day, the M-AWS travelled towards the slope of the Dome A, on the opposite side of the saddle from Dome F. The SAT reproduced in ERA5 on 14 Jan 2019 at 00:00 UTC is similar to that of 12 Jan 2019 at 00:00 UTC, with cold SAT extending slightly to the north with respect to the previous case (Fig. 5c). However, that night was characterized by very cold temperatures that reached -40 ˚C at the M-AWS, -37.3 ˚C at Dome Fuji and -34.5 ˚C at JASE2007. Temperatures in ERA5 were overestimated at all the AWS locations with a bias between 1.7 and 3.4 ˚C. Nonetheless, the horizontal gradient between the M-AWS and the Dome Fuji remained below 1 ˚C 100km^{-1} in both observations and reanalysis.

17-18 and 18-19 Jan 2019

During the following days the 500 hPa anticyclone coupled to another mid-latitude ridge coming from Enderby Land, leaving the Dome F in a transition area with temperatures ranging from -30 to -36 ˚C at 500 hPa (Fig. S4d). The SAT reproduced in ERA5 on the 17-18 Jan 2019 night around the top of the dome was higher than the previous 13-14 night (Fig. 5d) probably due to the cloudy and foggy conditions of that night as recorded on the in-situ weather reports (Fig. 4).

When the sky cleared on 18-19, the SAT fell to values similar to previous case studies. During these two nights, the M-AWS was located at the eastern side of the saddle. Despite being relatively close to Dome Fuji station (101 km), M-AWS measured minimum temperatures of -37.3 ˚C and -40.8 ˚C in the first and the second night respectively, while Dome F measured -34.7 ˚C and -36.9 ˚C. This makes a gradient of 1.3 ˚C 100km^{-1} in the first night and 2.0 ˚C 100km^{-1} in the second one. This case, like the one of 7 Jan 2019, suggests that the sides of the saddle accumulate the cold air from the cool pool that descends from the saddle and nearby domes. This dynamic is barely captured by ERA5 that presents much larger biases at M-AWS compared to Dome Fuji.

5.2 Temperature gradients during less stable conditions

Stable conditions with low wind speeds at Dome Fuji dominated during the campaign. However, few events occurred with less stable conditions associated with strong flow or temperature advections. We discuss two of these events below.

14-17 Jan 2019

From 14 to 17 Jan 2019 a 500 hPa anticyclone centred in the south of Dome F moved NE generating a strong flow over the study area (Fig. 6a,c,e). Initially, it advected warm and moist air from the Enderby Land over the Dome F (Fig. 7a), also evidenced by the counter clockwise rotation of the wind with height at 16 Jan 2019 00 UTC (Fig. S6). However from 16 to 17 Jan 2019, the flow direction became almost parallel to the isotherms stopping the advection (Fig. 6e). The strong synoptic flow suppressed the downslope winds over the dome during those days. The wind direction shifted gradually from NE to NW (Fig. 4). Advection was observed at Dome Fuji station with a large increase in the nocturnal SAT, rising 6.5 ˚C on the night of 14-15 Jan 2019 with respect to the previous night and reducing the diurnal temperature variation at the station (Table 2 and Fig. 4). The rise of the SAT is lower in ERA5 with only 4.0 ˚C. It is noticeable that ERA5 simulated an increase in SAT at JASE2007 while the observations showed a decrease. The rise at JASE2007 occurred the following night. In contrast, M-AWS, located on the saddle, presented modest increases in the minimum SAT during the first two nights. These colder conditions over the saddle are well represented in ERA5 (Fig. 6b,d). On the night from 16 to 17 Jan 2019 the SAT over the M-AWS location suddenly rose under the NW flow. The SAT of the region became quite homogenous on 17 Jan as observed at the three AWS and in the reanalysis (Fig. 6f). ERA5 succeeded to simulate the warmer temperatures on the saddle region. The temperature increase in this region is probably related to the advection of humidity (Fig. 7c) that produced fog in the region as indicated in the reports of meteorological observations (Fig. 4).

The biases between observations and reanalysis during this event are comparable with those calculated in a stable atmosphere. The horizontal gradients of the simulated SAT are larger than those observed during the two first nights when the gradients observed over the area are large. However, during the last night, when the SAT over the area is mostly homogenous and gradients are small, the simulated gradient are close to those observed.

18-21 Jan 2019

On 19 Jan 2019 a deep mid-latitude 500 hPa ridge stretched southward advecting cold air over the study area on the night of 19-20 Jan (Fig. 8a,b). Over the next several hours, a cut-off high formed west of Dome F driving a SE flow that brought low temperatures to the dome (Video S1 and S2). This is observed in Fig. 4 which shows a remarkable reduction in the maximum SAT at both M-AWS and Dome Fuji station. As discussed in the previous section, temperatures on 18-19 Jan night were much lower at the M-AWS position on the eastern side of the saddle than at Dome Fuji station (Table 2). Interestingly, SAT at the M-AWS increased on 19-20 Jan night, from -40.8 to -39.1 ˚C, while SAT at Dome Fuji decreased from -36.9 to -38.5 ˚C. This reduced the horizontal temperature gradient from 2.0 to 0.4 ˚C $100km^{-1}$. ERA5 simulated a decrease in the SAT on the saddle and an increase at Dome Fuji while it failed on reproduce the SAT distribution, showing lower temperatures on the dome than on the saddle (Fig. 8b). This resulted in a large error in the reanalysis horizontal gradient. This suggest that even a moderate flow can form a low-level cold pool flowing to the saddle. These situations are difficult to represent for ERA5 as observed in the cross section of that day (Fig. S9b). On the contrary, over the dome ridge ERA5 improves the representation of the gradient between Dome Fuji and JASE2007 with respect to the depression, due to the better representation of the JASE2007 temperature on the 19-20 night.

5.3 Mesoscale warm eddies near the dome

In periods without major advections, some anticyclonic eddies with a warm core are simulated in the evening near the Dome F in the ERA5 reanalysis. In Fig. 9 we present two examples. According to the ERA5 reanalysis during the period of study, these eddies commonly form over the dome and on the east slopes, and only occasionally over the west and north slopes. Unfortunately, the M-AWS did not cross any of those and we cannot verify if they are accurately simulated or are an artifact of the reanalysis, but we report them in this section as a structure for further investigation in future research. A visual inspection of the reanalyses in June and July 2019 over the whole eastern ice sheet reveals that it is not a summer only feature, but it is present as well in winter. Furthermore, more than one eddy can be present over different parts of the plateau at the same time. In summer, there are one or two anticyclonic eddies simultaneously over the plateau and only occasionally three, while in winter it is common to have one eddy near each dome (Fig. S11).

The warm core of the anticyclonic eddies simulated by ERA5 is small, with a radius of about 50 km, on the meso-β scale, and sometimes elongated. The streamlines begin at the core of the eddies being the “origin of the horizontal wind” over the ice sheet according the reanalysis. These anticyclonic eddies in summer are more evident at 21 UTC when the temperature gradients are strongest, probably due the onset of the nocturnal diabatic cooling. The gradient between the core and the outside of the eddies can reach *ca.* 5 ˚C in 100 km during the strongest moments of the day.

We examined the vertical structure of the eddy simulated by ERA5 over the Dome Fuji on 7 Jan 2019 at 21:00 UTC (Fig. 10). Areas outside the eddy core show a relatively strong surface inversion with *ca.* 100 m depth. In these areas, the difference between the temperature of the surface level and the top level of the inversion ground layer are greater than 5 ˚C (see Fig. 10 between 30˚ - 35˚ or 45˚ - 50˚). The top of the surface inversion layer folds down at the core of the eddy, descending to *ca.* 120 m high, and the difference between the surface-level temperature and the top level of the inversion ground layer decreases to 2-3 ˚C. The inversion gradients in the core of the eddy are similar than those found using radiosonde data in January at Dome C (Tomasi et al., 2011).

According ERA5, the eddy modifies the stability of the low atmosphere below 100 m height showing a notable reduction of the lapse rate of the potential temperature into the warm core indicating a weakened static stability (Fig. 10). Above 100 m, the lapse rate is mainly regulated by the strength of the subsidence. This results may explain the less stable thermodynamic conditions found at Dome C with respect the South Pole (Hagelin et al., 2008). However, the warm air over the cold terrain may increase the surface static stability on the few first meters over the ground which may be not well described in the vertical resolution of the state-of-the-art reanalysis. Reanalysis are likely not to perfectly reproduce these mesoscale structures, especially near-ground conditions as noted in previous sections. Further investigation and in-situ measurements are needed to formally report the presence and thermal features of these structures.

6. Discussion and Conclusions

Most of the atmospheric studies in the Antarctic Plateau are based on vertical analyses of the boundary layer or long-term climatology using the few weather stations available in the region. There is a lack of studies examining the horizontal mesoscale meteorological features of the Eastern Plateau on a daily scale, in part due to the lack of in-situ meteorological observations. In this article, we take advantage of the temperature data we obtained by the M-AWS over the Dome F. Thanks to this expedition we were able to measure temperature gradients and characterize the mesoscale dynamics and temperature gradients of the Eastern Antarctic Plateau near Dome F in the 2018-19 summer, when the YOPP-SH SOP was conducted. We investigate the capacity of the state-of-the-art reanalyses to reproduce the daily variations of SAT in different parts of the plateau and the reliability of the gradients simulated in the region.

Although the analysis presented here is limited by the number of in-situ observations over the area and the possible overestimation of some daytime temperatures recorded in the AWS, the combination of reanalysis and AWS observations during 43 days is sufficient to face a first characterization of the variations of the summertime nocturnal SAT and the near-surface circulation that affects the SAT. Here, we report (1) observations of possible cold pools not well reproduced by the ERA5 analysis, (2) large temperature variations affecting unevenly the dome and (3) the possible existence of surface meso-β eddies with warm cores with horizontal gradients over 5 ˚C $100km^{-1}$ simulated by ERA5. Some of these characteristics are schematically represented in Fig. 11 with the warm-core eddies at the top of the dome and the recurrent areas of cold pools over the saddle point.

After an evaluation of three reanalysis we found that ERA5 is the best performing in the region, with MERRA-2 very close to it. Those two reanalysis performs much better than ERA-Interim. However, it is not possible to discern that part of the improvements in surface temperature representation is due to the better resolution of the ERA5 with respect to ERA-Interim or to the additional reprocessed datasets and the improved parametrizations of the new reanalysis. A detailed analysis of the weather events between 7 and 22 Jan 2019 provides information of the reliability of the reanalysis, such as ERA5, over the Antarctic Plateau in summer. We found that nigh-time meso-α gradients (200-500 km) are very variable day to day depending on the synoptic conditions, and their changes are not consistently reproduced by ERA5. In general, ERA5 tends to underestimate thermal horizontal gradients and fails to reproduce some possible cold pools over depressed areas of the terrain. The SAT gradients over the plateau simulated by ERA5 are more reliable when they are weak and under stable conditions. The data presented here complements climatological evaluations of reanalysis such as presented by Gossart et al. (2019) and help to interpret their performance over the Antarctic Ice Sheet. Moreover, a better understanding of small-scale features that cause inhomogeneous snow accumulation and snow redistribution can also help to interpret the variability of the surface mass balance in areas of the interior of the Antarctic ice sheet (Kameda et al., 2008) and the ice cores obtained there.

Since daily temperature variations have effects on atmospheric transparency on the domes, our findings are also of interest for astronomical observation campaigns in the region (Lawrence, 2004). In particular, the warm core of the meso-β eddies identified in the ERA5 reanalysis may contribute to change the turbulence regimes. These eddies are observed to occur in ERA5 more frequently at the top of the domes, where several telescopes are located (Hagelin et al., 2008) and occasionally moves towards the slopes of the dome or disappear according the synoptic regime. On the one hand the warm air near to the cold terrain may increase the surface static stability in the few first meters, on the other, the weaker inversion aloft reduces the stable stratification. The height of the stratified layer into these structures with respect the height of the telescope may have a large impact on the astronomical seeing of the Antarctic observatories. The observational report and the study of the atmospheric conditions over the dome during these events is out of the scope of this study, however, due to their potential implications for astronomical observations, these phenomena must be studied in more detail. Determining the presence or absence of a meso-β eddie at an observatory site also illustrates the importance of forecasting and monitoring the weather to improve the scheduling of astronomical activities.

This study, developed after a short campaign in the Antarctic summer, provide a first look of the small-scale dynamics of the Antarctic Plateau. The development of a dense network such as the Antarctic Meteorological Research Center operates in the Ross Ice Shelf and West Antarctic Ice Sheet (Lazzara et al. 2012) can provide a more detailed picture on the small-scale near-surface dynamics of the East Antarctic Plateau. However, to do this, AWS must be distributed not only on the ridges, such as in previous investigations, but more evenly balanced, covering both the ridges and the depressions of the terrain around the dome.

Acknowledgments

This is a contribution to the Year of Polar Prediction (YOPP), a flagship activity of the Polar Prediction Project (PPP), initiated by the World Weather Research Programme (WWRP) of the World Meteorological Organization (WMO). The authors acknowledge the computer resources, technical expertise and assistance provided by the Centro de Computación Científica at the Universidad Autónoma de Madrid (CCC-UAM). We especially thank the help of Manolo Bañon in the design of the M-AWS and his very valuable contribution preparing the data for this paper. We thank Shuji Fujita for the data of Japanese stations, and George Weidner and Matthew Lazzara and his team for the interesting discussions about measurements on the Antarctic Plateau, which helped to improve this article. We want to acknowledge J.A. Higuera and J. González from SEGAINVEX-UAM and R. Vicente from AEMET, and expedition members R. Larramendi, H. Moreno, I. Oficialdegui and M. Olivera for their contribution to the project. We thanks the two anonymous reviewers for their constructive comments that helped to improve this paper.

Funding Sources

This work was supported by the Spanish Agencia Estatal de Investigación (AEI) and Fondo Europeo al Desarrollo Regional (FEDER) through the MICROAIRPOLAR project [grant number CTM2016-79741-R] and the Generalitat de Catalunya through the ANTALP Research Group [grant number 2017 SGR 1102].

Author contribution

Sergi Gonzalez: Conceptualization, Investigation, Writing-Original draft preparation. Francisco Vasallo: Conceptualization, Investigation, Writing – Review & Editing. Pablo Sanz: Conceptualization, Data curation, Writing – Review & Editing. Antonio Quesada: Conceptualization, Supervision, Funding acquisition, Writing – Review & Editing. Ana Justel: Conceptualization, Data curation, Formal analysis, Supervision, Funding acquisition, Writing-Original draft.

References

Allison, I., Wendler, G., Radok, U., 1993. Climatology of the east Antarctic Ice Sheet (100°E to 140°E) derived from automatic weather stations. J. Geophys. Res. Atmos. 98, 8815–8823. https://doi.org/10.1029/93JD00104

Argentini, S., Viola, A., Sempreviva, A.M., Petenko, I., 2005. Summer boundary-layer height at the plateau site of Dome C, Antarctica. Boundary-Layer Meteorol. 115, 409–422. https://doi.org/10.1007/s10546-004-5643-6

Atlaskin, E., Vihma, T., 2012. Evaluation of NWP results for wintertime nocturnal boundary-layer temperatures over Europe and Finland. Q. J. R. Meteorol. Soc. 138, 1440–1451. https://doi.org/10.1002/qj.1885

Bracegirdle, T.J., Marshall, G.J., 2012. The reliability of antarctic tropospheric pressure and temperature in the latest global reanalyses. J. Clim. 25, 7138–7146. https://doi.org/10.1175/JCLI-D-11-00685.1

Bromwich, D.H., Werner, K., Casati, B., Powers, J.G., Gorodetskaya, I. V., Massonnet, F., Vitale, V., Heinrich, V.J., Liggett, D., Arndt, S., Barja, B., Bazile, E., Carpentier, S., Carrasco, J.F., Choi, T., Choi, Y., Colwell, S.R., Cordero, R.R., Gervasi, M., Haiden, T., Hirasawa, N., Inoue, J., Jung, T., Kalesse, H., Kim, S.-J., Lazzara, M.A., Manning, K.W., Norris, K., Park, S.-J., Reid, P., Rigor, I., Rowe, P.M., Schmithüsen, H., Seifert, P., Sun, Q., Uttal, T., Zannoni, M., Zou, X., 2020. The Year of Polar Prediction in the Southern Hemisphere (YOPP-SH). Bull. Am. Meteorol. Soc. preprint, 1–56. https://doi.org/10.1175/bams-d-19-0255.1

Chen, C., Liu, L.-M., 1993. Joint Estimation of Model Parameters and Outlier Effects in Time Series. J. Am. Stat. Assoc. 88, 284. https://doi.org/10.2307/2290724

Dabberdt, W.F., 1970. A Selective Climatology of Plateau Station, Antarctica. J. Appl. Meteorol. 9, 311–315. https://doi.org/10.1175/1520-0450(1970)009<0312:ascops>2.0.co;2

Dee, D.P., Balmaseda, M., Balsamo, G., Engelen, R., Simmons, A.J., Thépaut, J.N., 2014. Toward a consistent reanalysis of the climate system. Bull. Am. Meteorol. Soc. 95, 1235–1248. https://doi.org/10.1175/BAMS-D-13-00043.1

Dee, D.P., Uppala, S.M., Simmons, A.J., Berrisford, P., Poli, P., Kobayashi, S., Andrae, U., Balmaseda, M.A., Balsamo, G., Bauer, P., Bechtold, P., Beljaars, A.C.M., van de Berg, L., Bidlot, J., Bormann, N., Delsol, C., Dragani, R., Fuentes, M., Geer, A.J., Haimberger, L., Healy, S.B., Hersbach, H., H??lm, E. V., Isaksen, L., K??llberg, P., K??hler, M., Matricardi, M., Mcnally, A.P., Monge-Sanz, B.M., Morcrette, J.J., Park, B.K., Peubey, C., de Rosnay, P., Tavolato, C., Th??paut, J.N., Vitart, F., 2011. The ERA-Interim reanalysis: Configuration and performance of the data assimilation system. Q. J. R. Meteorol. Soc. 137, 553–597. https://doi.org/10.1002/qj.828

ECMWF, 2009. IFS Documentation CY33R1 - Part IV: Physical Processes, in: IFS Documentation CY33R1, IFS Documentation. ECMWF, Reding, England, p. 162.

Enomoto, H., Motoyama, H., Shiraiwa, T., Saito, T., Kameda, T., Furukawa, T., Takahashi, S., Kodama, Y., Watanabe, O., 1998. Winter warming over Dome Fuji, East Antarctica and semiannual oscillation in the atmospheric circulation. J. Geophys. Res. Atmos. 103, 23103–

23111. https://doi.org/10.1029/98JD02001

Fréville, H., Brun, E., Picard, G., Tatarinova, N., Arnaud, L., Lanconelli, C., Reijmer, C., Van Den Broeke, M., 2014. Using MODIS land surface temperatures and the Crocus snow model to understand the warm bias of ERA-Interim reanalyses at the surface in Antarctica. Cryosphere 8, 1361–1373. https://doi.org/10.5194/tc-8-1361-2014

Gallée, H., Gorodetskaya, I. V., 2010. Validation of a limited area model over Dome C, Antarctic Plateau, during winter. Clim. Dyn. 34, 61–72. https://doi.org/10.1007/s00382-008-0499-y

Gelaro, R., McCarty, W., Suárez, M.J., Todling, R., Molod, A., Takacs, L., Randles, C.A., Darmenov, A., Bosilovich, M.G., Reichle, R., Wargan, K., Coy, L., Cullather, R., Draper, C., Akella, S., Buchard, V., Conaty, A., da Silva, A.M., Gu, W., Kim, G.K., Koster, R., Lucchesi, R., Merkova, D., Nielsen, J.E., Partyka, G., Pawson, S., Putman, W., Rienecker, M., Schubert, S.D., Sienkiewicz, M., Zhao, B., 2017. The modern-era retrospective analysis for research and applications, version 2 (MERRA-2). J. Clim. 30, 5419–5454. https://doi.org/10.1175/JCLI-D-16-0758.1

Genthon, C., Six, D., Favier, V., Lazzara, M., Keller, L., 2011. Atmospheric temperature measurement biases on the Antarctic plateau. J. Atmos. Ocean. Technol. 28, 1598–1605. https://doi.org/10.1175/JTECH-D-11-00095.1

Genthon, C., Town, M.S., Six, D., Favier, V., Argentini, S., Pellegrini, A., 2010. Meteorological atmospheric boundary layer measurements and ECMWF analyses during summer at Dome C, Antarctica. J. Geophys. Res. Atmos. 115, D05104. https://doi.org/10.1029/2009JD012741

Gonzalez, S., Banon, M., Albero, J. V., Larramendi, R., Moreno, H., Vasallo, F., Sanz, P., Quesada, A., Justel, A., 2019. Weather observations of remote polar areas using an AWS onboard a unique zero-emissions polar vehicle. Bull. Am. Meteorol. Soc. 100, 1891–1895. https://doi.org/10.1175/BAMS-D-19-0110.1

Gossart, A., Helsen, S., Lenaerts, J.T.M., Vanden Broucke, S., van Lipzig, N.P.M., Souverijns, N., 2019. An evaluation of surface climatology in state-of-the-art reanalyses over the Antarctic Ice Sheet. J. Clim. 32, 6899–6915. https://doi.org/10.1175/JCLI-D-19-0030.1

Hagelin, S., Masciadri, E., Lascaux, F., Stoesz, J., 2008. Comparison of the atmosphere above the south pole, dome C and dome A: First attempt. Mon. Not. R. Astron. Soc. 387, 1499–1510. https://doi.org/10.1111/j.1365-2966.2008.13361.x

Hakim, G.J., Bumbaco, K.A., Tardif, R., Powers, J.G., 2020. Optimal network design applied to monitoring and forecasting surface temperature in Antarctica. Mon. Weather Rev. 148, 857–873. https://doi.org/10.1175/MWR-D-19-0103.1

Hersbach, H., Bell, B., Berrisford, P., Hirahara, S., Horányi, A., Muñoz-Sabater, J., Nicolas, J., Peubey, C., Radu, R., Schepers, D., Simmons, A., Soci, C., Abdalla, S., Abellan, X., Balsamo, G., Bechtold, P., Biavati, G., Bidlot, J., Bonavita, M., De Chiara, G., Dahlgren, P., Dee, D., Diamantakis, M., Dragani, R., Flemming, J., Forbes, R., Fuentes, M., Geer, A., Haimberger, L., Healy, S., Hogan, R.J., Hólm, E., Janisková, M., Keeley, S., Laloyaux, P., Lopez, P., Lupu, C., Radnoti, G., de Rosnay, P., Rozum, I., Vamborg, F., Villaume, S., Thépaut, J.N., 2020. The ERA5 global reanalysis. Q. J. R. Meteorol. Soc. 146, 1999–2049. https://doi.org/10.1002/qj.3803

Hirasawa, N., Nakamura, H., Motoyama, H., Hayashi, M., Yamanouchi, T., 2013. The role of synoptic-scale features and advection in prolonged warming and generation of different forms of precipitation at Dome Fuji station, Antarctica, following a prominent blocking event. J. Geophys. Res. Atmos. 118, 6916–6928. https://doi.org/10.1002/jgrd.50532

Hudson, S.R., Brandt, R.E., 2005. A look at the surface-based temperature inversion on the Antarctic Plateau. J. Clim. 18, 1673–1696. https://doi.org/10.1175/JCLI3360.1

Jones, P.D., Lister, D.H., 2015. Antarctic near-surface air temperatures compared with ERA-Interim values since 1979. Int. J. Climatol. 35, 1354–1366. https://doi.org/10.1002/joc.4061

Jung, T., Gordon, N.D., Bauer, P., Bromwich, D.H., Chevallier, M., Day, J.J., Dawson, J., Doblas-Reyes, F., Fairall, C., Goessling, helge F., Holland, M., Inoue, J., Iversen, T., Klebe, St., Lemke, P., Losch, M., Makshtas, A., Mills, B., Nurmi, P., Perovich, D., Reid, P., Renfrew, I.A., Smith, G., Svensson, G., Tolstykh, M., Yang, Q., 2016. Advancing polar prediction capabilities on daily to seasonal time scales. Bull. Am. Meteorol. Soc. 97, 1631–1647. https://doi.org/10.1175/BAMS-D-14-00246.1

Kameda, T., Motoyama, H., Fujita, S., Takahashi, S., 2008. Temporal and spatial variability of surface mass balance at Dome Fuji, East Antarctica, by the stake method from 1995 to 2006. J. Glaciol. 54, 107–116. https://doi.org/10.3189/002214308784409062

Kikuchi, T., Satow, K., Ohata, T., Yamanouchi, T., Nishio, F., 1992. Wind and temperature regime in mizuho plateau, East Antarctica. Int. J. Remote Sens. 13, 67–79. https://doi.org/10.1080/01431169208904026

Lawrence, J.S., 2004. Infrared and Submillimeter Atmospheric Characteristics of High Antarctic

Plateau Sites. Publ. Astron. Soc. Pacific 116, 482–492. https://doi.org/10.1086/420757

López-de-Lacalle, J., 2019. Package “tsoutliers”. Detection of Outliers in Time Series. https://doi.org/10.2307/2290724

Markus, T., Neumann, T., Martino, A., Abdalati, W., Brunt, K., Csatho, B., Farrell, S., Fricker, H., Gardner, A., Harding, D., Jasinski, M., Kwok, R., Magruder, L., Lubin, D., Luthcke, S., Morison, J., Nelson, R., Neuenschwander, A., Palm, S., Popescu, S., Shum, C.K., Schutz, B.E., Smith, B., Yang, Y., Zwally, J., 2017. The Ice, Cloud, and land Elevation Satellite-2 (ICESat-2): Science requirements, concept, and implementation. Remote Sens. Environ. 190, 260–273. https://doi.org/10.1016/j.rse.2016.12.029

Navarro-Serrano, F., López-Moreno, J.I., Azorin-Molina, C., Alonso-González, E., Tomás-Burguera, M., Sanmiguel-Vallelado, A., Revuelto, J., Vicente-Serrano, S.M., 2018. Estimation of near-surface air temperature lapse rates over continental Spain and its mountain areas. Int. J. Climatol. 38, 3233–3249. https://doi.org/10.1002/joc.5497

Parish, T.R., Bromwich, D.H., 2007. Reexamination of the Near-Surface Airflow over the Antarctic Continent and Implications on Atmospheric Circulations at High Southern Latitudes*. Mon. Weather Rev. 135, 1961–1973. https://doi.org/10.1175/MWR3374.1

Parish, T.R., Cassano, J.J., 2003. The role of katabatic winds on the Antarctic surface wind regime. Mon. Weather Rev. 131, 317–333. https://doi.org/10.1175/1520-0493(2003)131<0317:TROKWO>2.0.CO;2

Scambos, T.A., Campbell, G.G., Pope, A., Haran, T., Muto, A., Lazzara, M., Reijmer, C.H., van den Broeke, M.R., 2018. Ultralow Surface Temperatures in East Antarctica From Satellite Thermal Infrared Mapping: The Coldest Places on Earth. Geophys. Res. Lett. 45, 6124–6133. https://doi.org/10.1029/2018GL078133

Surdyk, S., 2002. Low microwave brightness temperatures in central Antarctica: Observed features and implications. Ann. Glaciol. 34, 134–140. https://doi.org/10.3189/172756402781817464

Takahashi, S., Kameda, T., Enomoto, H., Shiraiwa, T., Kodama, Y., Fujita, S., Motoyama, H., Watanabe, O., Weidner, G.A., Stearns, C.R., 1998. Automatic weather station program during Dome Fuji project by JARE in east Dronning Maud Land, Antarctica. Ann. Glaciol. 27, 528–534. https://doi.org/10.3189/1998AoG27-1-528-534

Tetzner, D., Thomas, E., Allen, C., 2019. A validation of ERA5 reanalysis data in the southern antarctic peninsula—Ellsworth land region, and its implications for ice core studies.

Geosciences 9, 289. https://doi.org/10.3390/geosciences9070289

Thompson, D.C., 1969. The coreless winter at Scott Base, Antarctica. Q. J. R. Meteorol. Soc. 95, 404–407. https://doi.org/10.1002/qj.49709540413

Tomasi, C., Petkov, B., Benedetti, E., Valenziano, L., Vitale, V., 2011. Analysis of a 4 year radiosonde data set at Dome C for characterizing temperature and moisture conditions of the Antarctic atmosphere. J. Geophys. Res. Atmos. 116. https://doi.org/10.1029/2011JD015803

Turner, J., Anderson, P., Lachlan-Cope, T., Colwell, S., Phillips, T., Kirchgaessner, A., Marshall, G.J., King, J.C., Bracegirdle, T., Vaughan, D.G., Lagun, V., Orr, A., 2009. Record low surface air temperature at Vostok station, Antarctica. J. Geophys. Res. Atmos. 114, 24102. https://doi.org/10.1029/2009JD012104

Van de Wiel, B.J.H., Moene, A.F., Jonker, H.J.J., Baas, P., Basu, S., Donda, J.M.M., Sun, J., Holtslag, A.A.M., 2012. The minimum wind speed for sustainable turbulence in the nocturnal boundary layer. J. Atmos. Sci. 69, 3116–3127. https://doi.org/10.1175/JAS-D-12-0107.1

van den Broeke, M.R., van Lipzig, N.P.M., 2003. Factors controlling the near-surface wind field in Antarctica. Mon. Weather Rev. 131, 733–743. https://doi.org/10.1175/1520-0493(2003)131<0733:FCTNSW>2.0.CO;2

Vignon, E., Hourdin, F., Genthon, C., Van de Wiel, B.J.H., Gallée, H., Madeleine, J.B., Beaumet, J., 2018. Modeling the Dynamics of the Atmospheric Boundary Layer Over the Antarctic Plateau With a General Circulation Model. J. Adv. Model. Earth Syst. 10, 98–125. https://doi.org/10.1002/2017MS001184

Vignon, E., van de Wiel, B.J.H., van Hooijdonk, I.G.S., Genthon, C., van der Linden, S.J.A., van Hooft, J.A., Baas, P., Maurel, W., Traullé, O., Casasanta, G., 2017. Stable boundary-layer regimes at Dome C, Antarctica: observation and analysis. Q. J. R. Meteorol. Soc. 143, 1241–1253. https://doi.org/10.1002/qj.2998

Yamanouchi, T., Hirasawa, N., Hayashi, M., Takahashi, S., Kaneto, S., 2003. Meteorological characteristics of Antarctic inland station, Dome Fuji (scientific paper). Mem. Natl. Inst. Polar Res. Spec. Issue 57, 94–104.

Zentek, R., Heinemann, G., 2020. Verification of the regional atmospheric model CCLM v5.0 with conventional data and lidar measurements in Antarctica. Geosci. Model Dev. 13, 1809–1825. https://doi.org/10.5194/gmd-13-1809-2020

Table 1. BIAS, mean absolute error (MAE) and Pearson correlation coefficient for performance comparison of ERA5, MERRA-2 and ERA-Interim reanalysis with the AWS observations during the campaign. In the top table using all hours, and in the bottom table using only the nocturnal hours (21, 00, 03 UTC).

	All hours								
	BIAS			**MAE**			**r-pearson**		
	ERA5	**MERRA-2**	**ERA-Interim**	**ERA5**	**MERRA-2**	**ERA-Interim**	**ERA5**	**MERRA-2**	**ERA-Interim**
M-AWS	-2.16	-2.54	1.11	3.25	3.30	3.10	0.82	0.83	0.85
DomeF	-2.44	-3.53	0.28	2.86	3.82	1.93	0.89	0.87	0.93
JASE	-1.59	-1.44	0.65	2.66	2.35	2.04	0.84	0.87	0.93
All AWS	-2.05	-2.49	0.66	2.91	3.16	2.33	0.84	0.84	0.89
	Night								
	BIAS			**MAE**			**r-pearson**		
	ERA5	**MERRA-2**	**ERA-Interim**	**ERA5**	**MERRA-2**	**ERA-Interim**	**ERA5**	**MERRA-2**	**ERA-Interim**
M-AWS	0.25	-0.14	3.52	2.19	1.89	4.03	0.81	0.85	0.79
DomeF	-0.80	-1.87	1.92	1.89	2.58	2.38	0.88	0.84	0.92
JASE	0.30	0.22	2.43	2.37	1.83	3.00	0.76	0.86	0.86
All AWS	-0.10	-0.59	2.57	2.15	2.10	3.09	0.81	0.83	0.84

Table 2. For selected nights, minimum SAT (ºC) and the corresponding horizontal SAT gradient (ºC $100km^{-1}$) observed at M-AWS, Dome Fuji and JASE2007 and simulated by ERA5.

	Observed			**ERA5**		
Temperature	**M-AWS**	**Dome Fuji**	**JASE2007**	**M-AWS**	**Dome Fuji**	**JASE2007**
6-7 Jan 2019	-38.0	-33.1	-35.2	-34.7	-34.5	-34.4
11-12 Jan 2019	-37.8	-36.1	-26.2	-37.0	-34.9	-29.2
13-14 Jan 2019	-40.0	-37.3	-34.5	-36.6	-35.6	-31.8
14-15 Jan 2019	-38.5	-30.8	-35.4	-35.8	-31.6	-30.8
15-16 Jan 2019	-36.7	-29.3	-30.8	-33.9	-29.4	-27.6
16-17 Jan 2019	-31.3	-32.6	-34.5	-28.6	-30.8	-31.8
17-18 Jan 2019	-37.3	-34.7	-30.9	-34.4	-33.6	-28.4
18-19 Jan 2019	-40.8	-36.9	-35.6	-37.0	-34.7	-28.9
19-20 Jan 2019	-39.1	-38.5	-39.0	-36.4	-37.1	-33.8

Gradient	**Dome Fuji - M-AWS**	**Dome Fuji - JASE2007**	**Dome Fuji - M-AWS**	**Dome Fuji - JASE2007**
6-7 Jan 2019	2.7	0.5	0.1	0.0
11-12 Jan 2019	0.7	-2.5	0.9	-1.5
13-14 Jan 2019	0.9	-0.7	0.3	-1.0
14-15 Jan 2019	2.6	1.2	1.4	-0.2
15-16 Jan 2019	2.5	0.4	1.5	-0.5
16-17 Jan 2019	-0.4	0.5	-0.7	0.3
17-18 Jan 2019	1.3	-1.0	0.4	-1.3
18-19 Jan 2019	2.0	-0.3	1.2	-1.5
19-20 Jan 2019	0.4	0.1	-1.1	-0.5

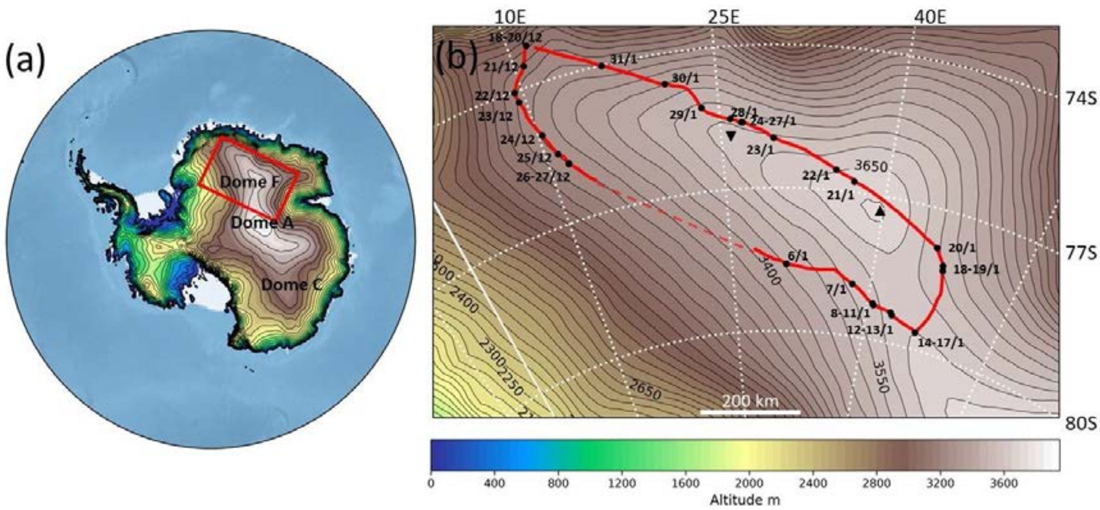

Figure 1. (a) Elevation map of the continent and position of the area of study. (b) Elevation map of the Area of study with the position of Dome Fuji station (▲), JASE2007 station (▼) and transect of the M-AWS and its space-time position during the 2018-19 campaign (●).

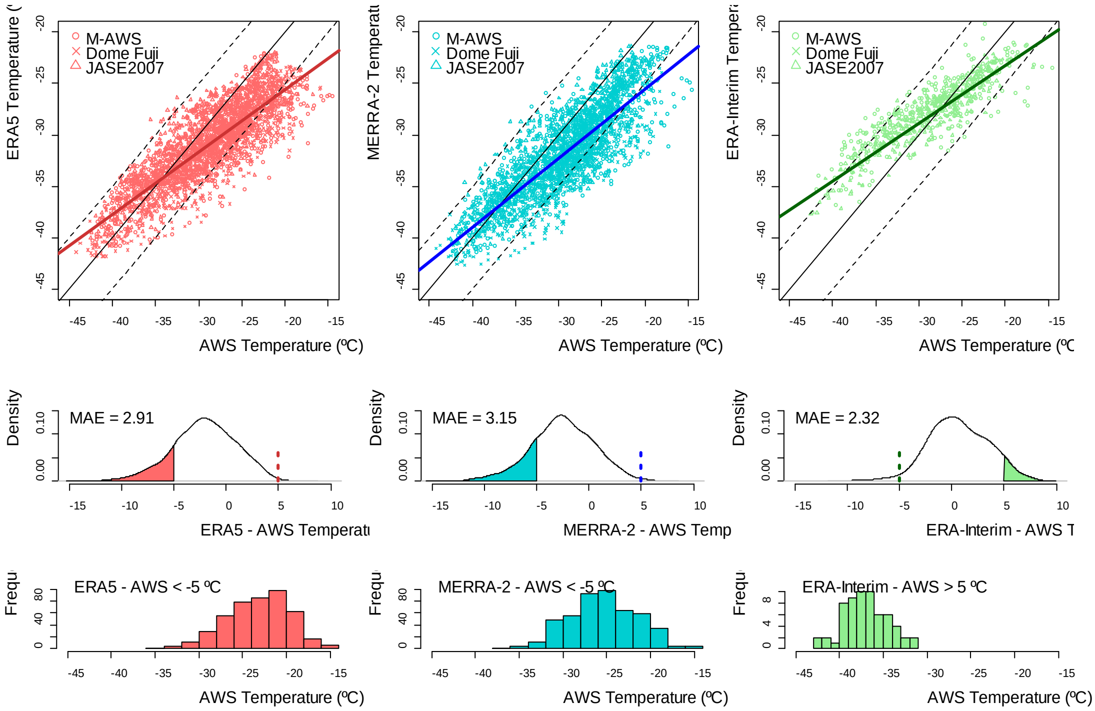

Figure 2. (a) A different scatterplot for each reanalysis, showing the temperature pairs provided by any of the AWSs and the corresponding reanalysis; the coloured lines are the least squares estimators of the linear regression models; solid black lines are the identities ones; and the dashed lines are the identity ±5 °C. (b) Distribution of bias sizes in ERA5, MERRA2 and ERA-Interim. (c) Frequency distribution of the temperatures observed in the AWSs when the sizes of the biases in ERA5 and MERRA2 are less than -5 °C and in ERA-Interim they are greater than 5 °C.

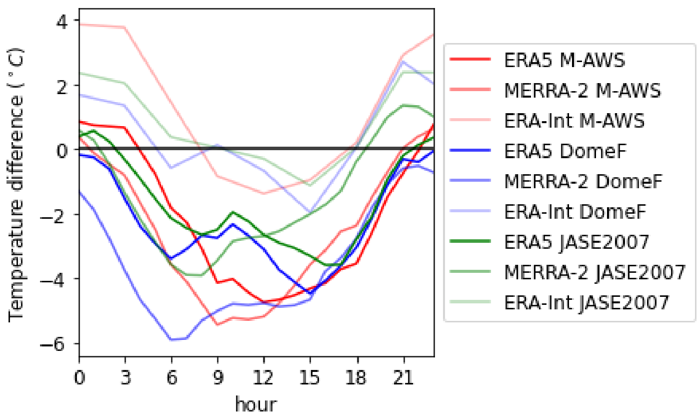

Figure 3. For each hour of the day, the averages of the differences between the temperatures calculated with each of the reanalyses and the observations recorded with each AWS are represented.

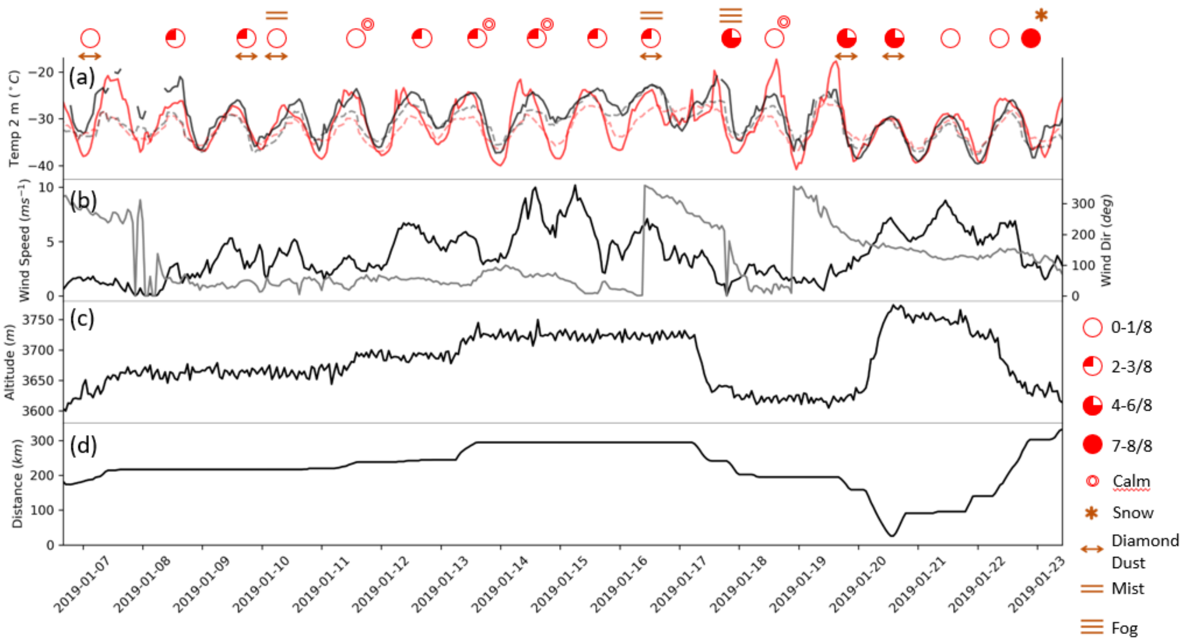

Figure 4. Time series of meteorological variables recorded during the campaign from 7 to 23 Jan 2019. (a) SAT observations at the M-AWS (red continuous line), at the Dome Fuji AWS (black continuous line) and the corresponding simulated by ERA5 (red and black dashed lines); and weather observations made during the transect at the M-AWS location. (b) Wind speed (black) and direction (grey) at Dome Fuji AWS. (c) Altitude of the M-AWS. (d) Distance between the M-AWS and Dome Fuji AWS.

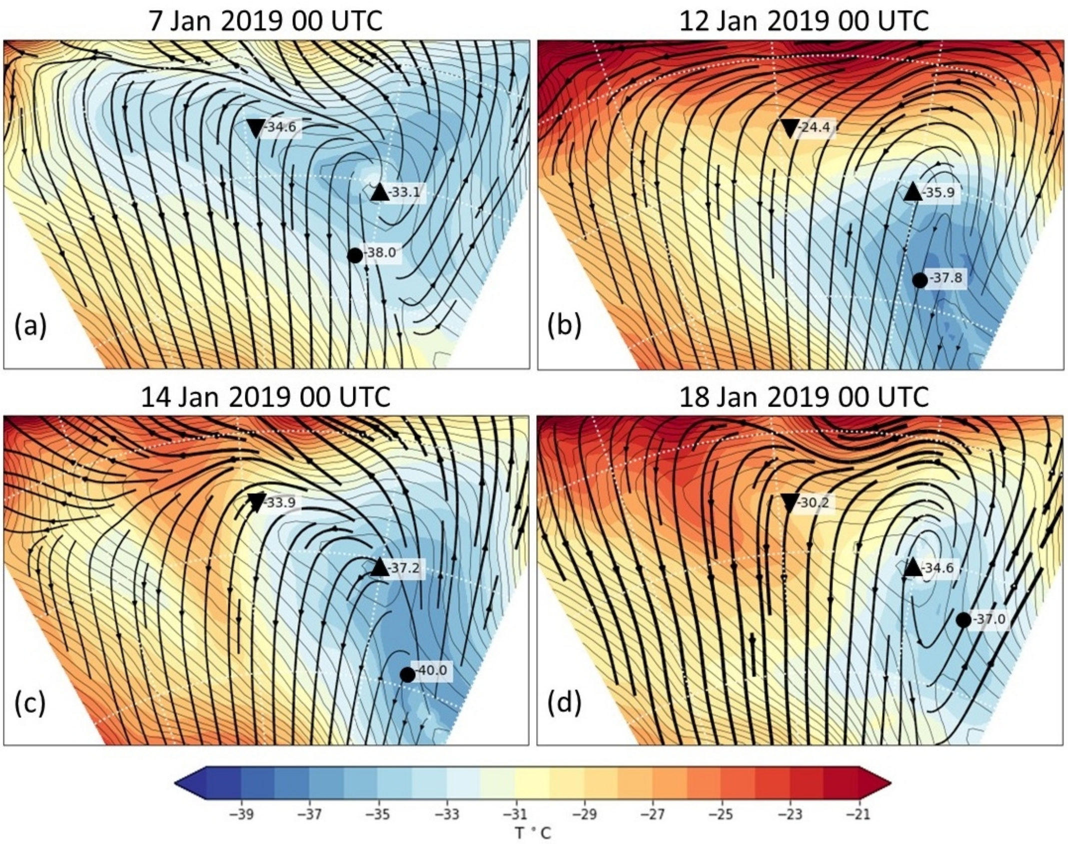

Figure 5. SAT simulated by ERA5 and observed at Dome Fuji (▲), JASE2007 (▼) and M-AWS (●) on (a) 7 Jan 2019 at 00:00 UTC, (b) 12 Jan 2019 at 00:00 UTC, (c) 14 Jan 2019 at 00:00 UTC and (d) 18 Jan 2019 00:00 UTC. Streamlines show the 10m wind simulated by ERA5 with thickness proportional to the wind speed. Thin isolines represent the topography of the terrain for reference.

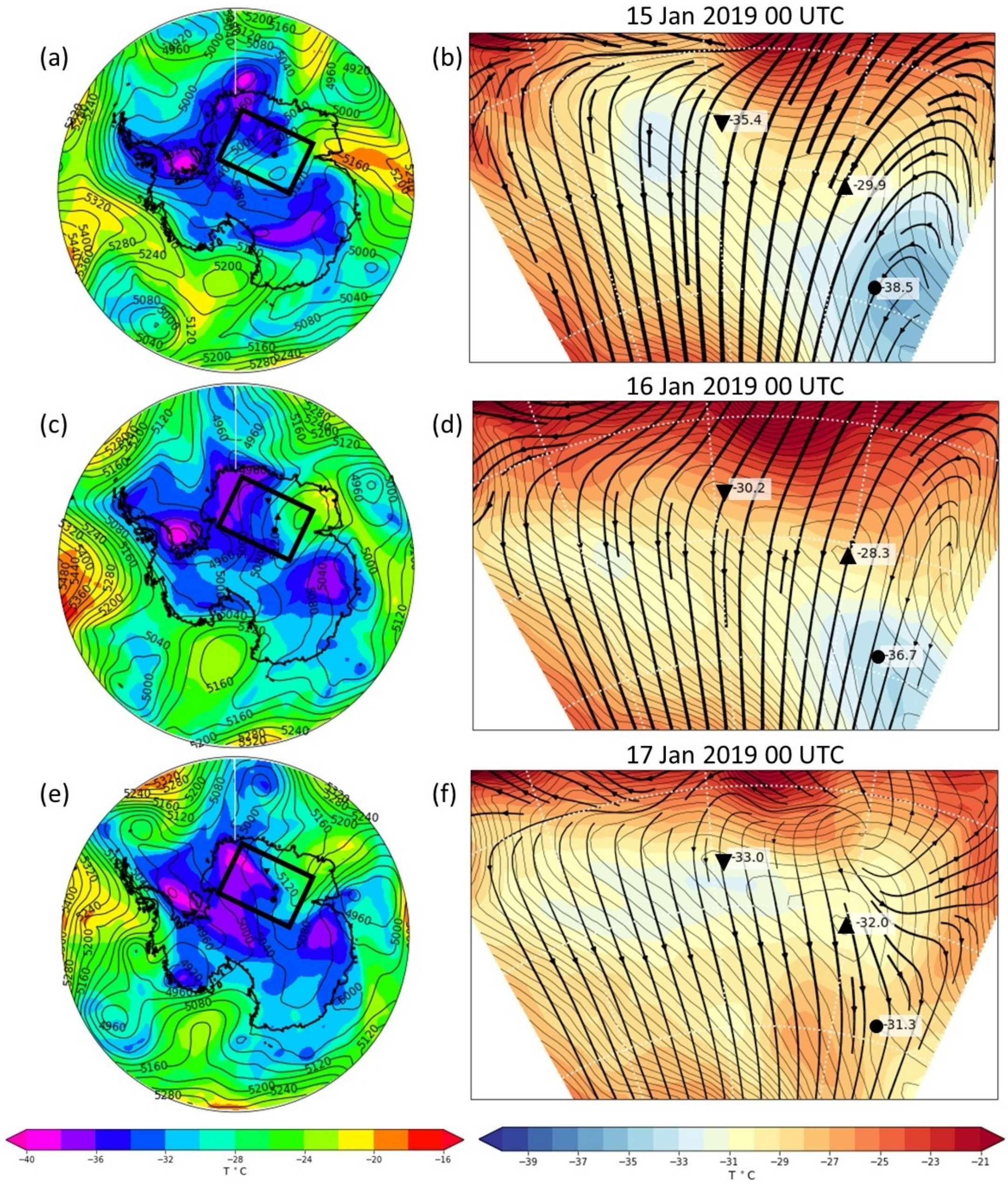

Figure 6. (a,c,e) Synoptic setting with temperature (shaded) and geopotential height (black lines) simulated by ERA5 at 500 hPa, and (b,d,f) SAT simulated by ERA5 and observed at Dome Fuji (▲), JASE2007 (▼) and M-AWS (●) on (a,b) 15 Jan 2019 at 00:00 UTC, (c,d) 16 Jan 2019 at 00:00 UTC, (e,f) 17 Jan 2019 at 00:00 UTC. Streamlines in (b),(d) and (f) show the 10m wind simulated by ERA5 with thickness proportional to the wind speed. Thin isolines represent the topography of the terrain for reference.

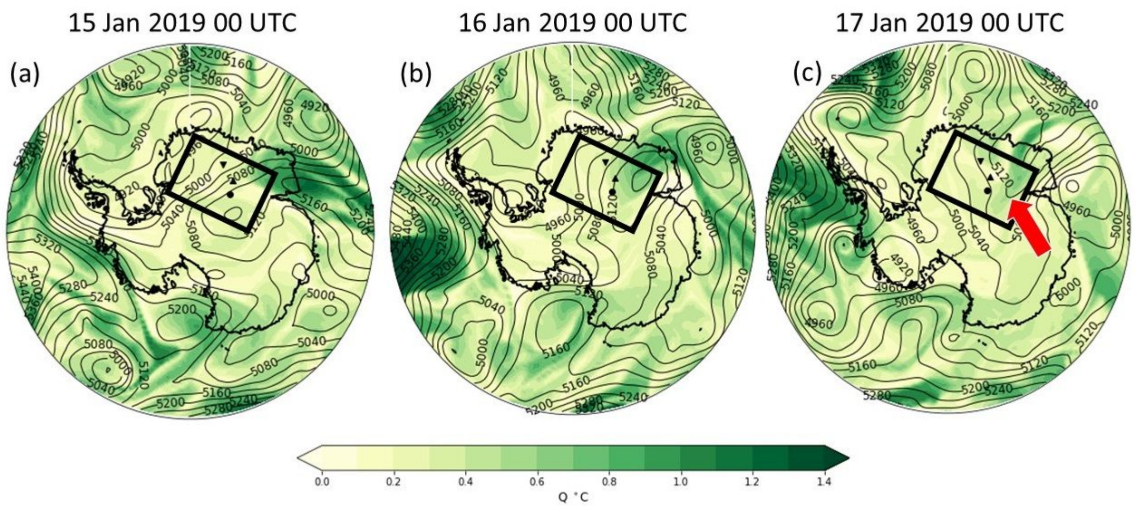

Figure 7. Specific humidity (shaded) and geopotential height (black lines) simulated by ERA5 at 500 hPa on (a) 15 Jan 2019 at 00:00 UTC, (b) 16 Jan 2019 at 00:00 UTC, (c) 17 Jan 2019 at 00:00 UTC. Dome Fuji (▲), JASE2007 (▼) and M-AWS (●). The arrow on (c) indicates the position of a band of humidity that could cause fog at M-AWS position on that day.

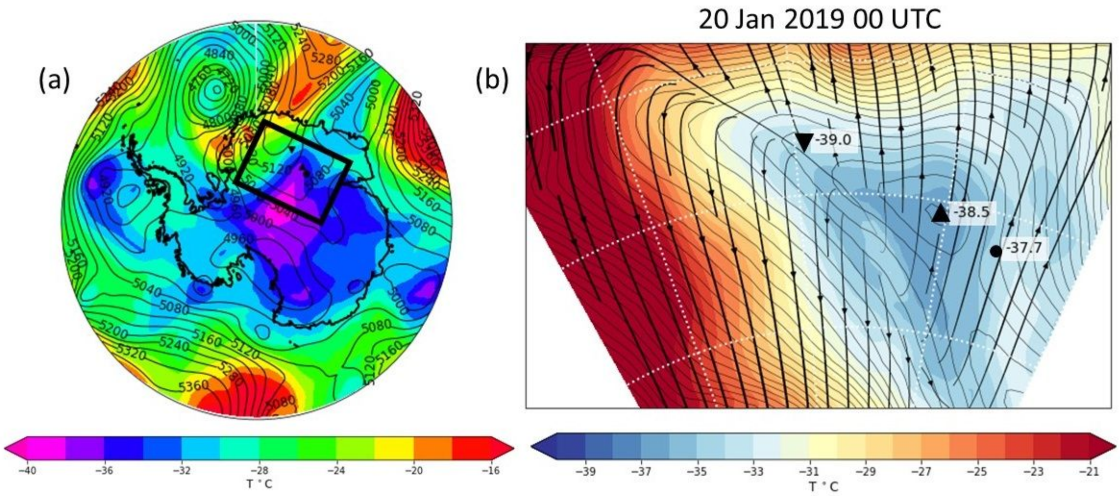

Figure 8. (a) Synoptic setting with temperature (shaded) and geopotential height (black lines) simulated by ERA5 at 500 hPa, and (b) SAT simulated by ERA5 and observed at Dome Fuji (▲), JASE2007 (▼) and M-AWS (●) on 20 Jan 2019 at 00:00 UTC. Streamlines in (b) show the 10m wind simulated by ERA5 with thickness proportional to the wind speed. Thin isolines represent the topography of the terrain for reference.

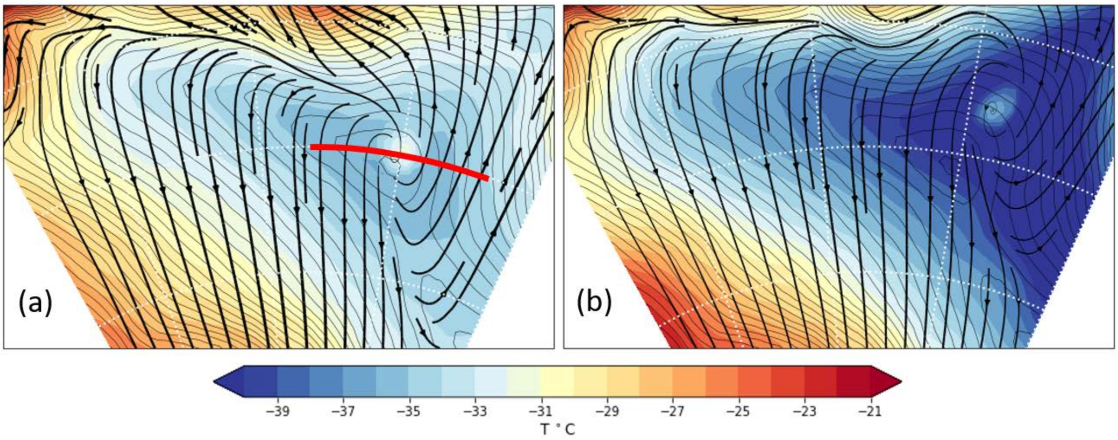

Figure 9. Examples of two anticyclonic eddies at Dome F. (a) 7 Jan 2019 at 21:00 UTC and (b) 27 Jan 2019 at 21:00. The red line on (a) indicates the cross section represented in Fig. 10. Streamlines show the 10m wind simulated by ERA5 with thickness proportional to the wind speed. Thin isolines represent the topography of the terrain for reference.

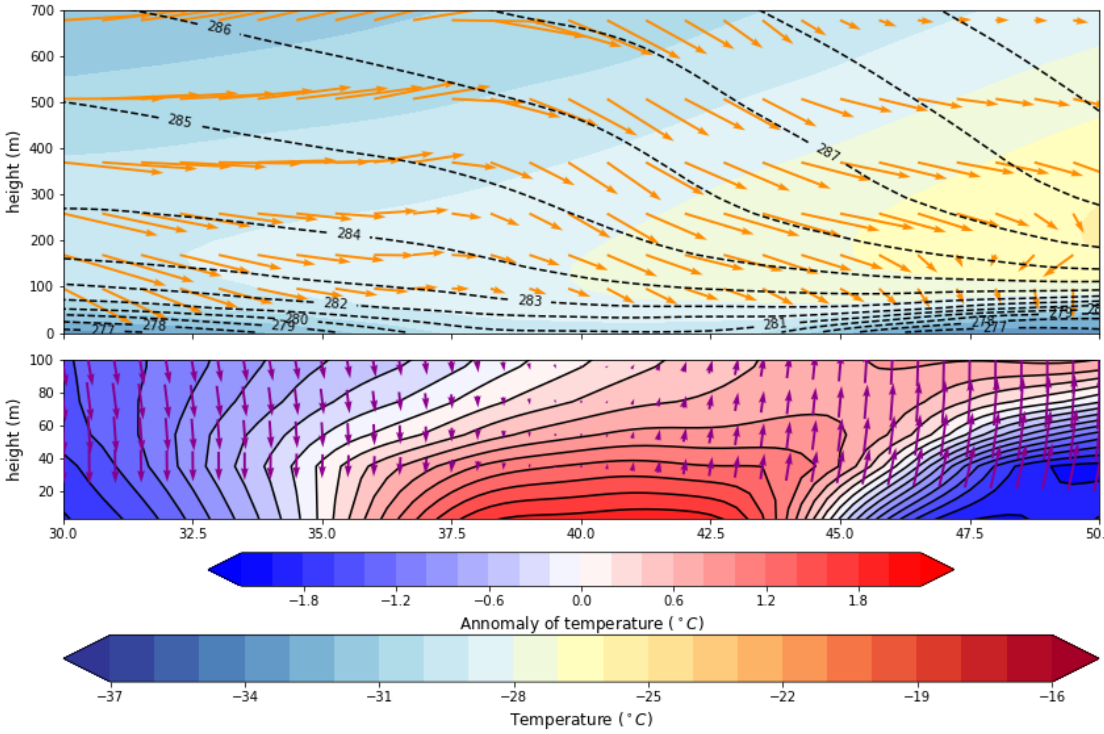

Figure 10. Cross sections of the anticyclonic mesoscale eddie shown in Fig. 9a on 7 Jan 2019. (a) Temperature (shaded), potential temperature (contours) and wind over the cross-section plane of the low atmosphere between 0 and 700m height. (b) Anomaly of temperature with respect the horizontal represented at the figure and horizontal wind of the low atmosphere between 0 and 100 m height.

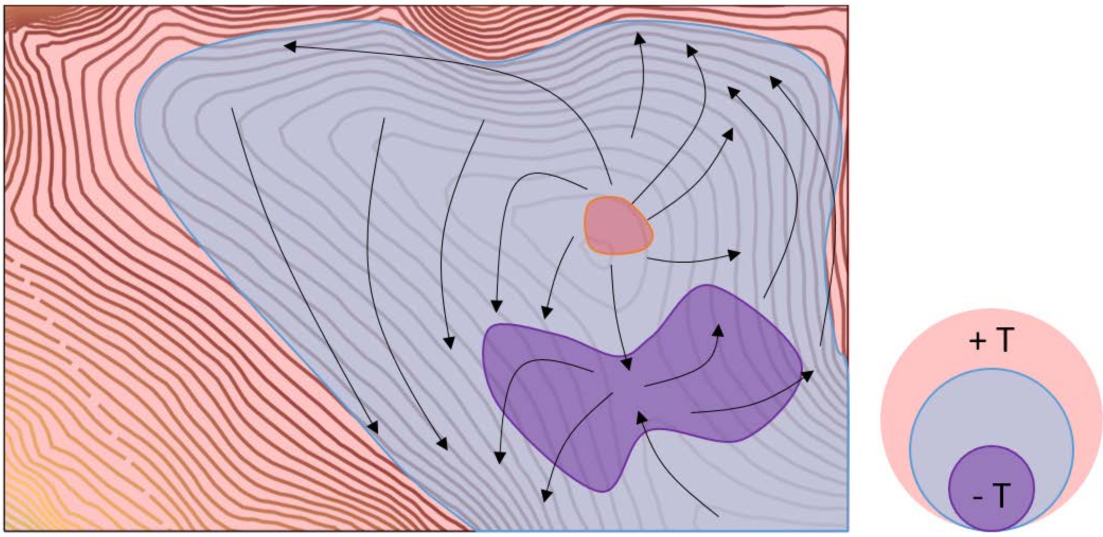

Figure 11. Conceptual model of some mesoscale structures analysed in this study. Note that the map do not reflect any particular day but features common at night found during the 6-week summer campaign. Isolines represent the topography shown in Figure 1b.